Solar-pumped passively Q-switched single crystal fiber lasers with several-nanosecond pulse width

ZIRUN LIU[1], YUANYUAN ZHANG[1], LANLING LAN[1,*], YAN LIU[1,*], JUNJUN TAN[2]
[1]*Center for Astronomy and Space Science, College of Mathematics and Physics, China Three Gorges University, Yichang, Hubei 443002, China*
[2]*College of Hydraulic and Environmental Engineering, China Three Gorges University, Yichang, Hubei 443002, China*

To achieve pulse output with several-nanosecond width of solar laser, a solar-pumped passively Q-switched laser (PQL) based on a short single crystal fiber (SCF) is proposed. The side-pumping of Nd:YAG SCF (Φ1 mm × 20 mm) can be achieved with a three-stage solar concentrator which consists of a rectangular parabolic mirror, a 2D-CPC and a 2V-shaped reflector. The solar power absorbed by the SCF can reach 40 W based on ray tracing with TracePro software. The output characteristics of SCF lasers are compared with different Q-switch elements (Cr^{4+}:YAG and V^{3+}:YAG). When the initial transmittance of Cr^{4+}:YAG and the output coupler reflectivity are 90% and 35%, the minimum output pulse width reaches 5.2 ns, which is less than that of the previously reported solar-pumped PQLs. This concentrator system and short SCF provide ideas for several-nanosecond pulse output generation of solar laser.

(Received December 30, 2024; accepted August 4, 2025)

Keywords: Solar pumped laser, Fiber laser, Passively Q-switched, Single crystal fiber, Solar concentrator

1. Introduction

Due to promising prospects in the fields of space debris removal, magnesium resource recycling, space optical communications, and space solar power stations, solar pumped lasers (SPLs) have attracted great interest [1-3]. SPLs have experienced rapid advancements in the past two decades. The laser output power has reached several hundred watts [4].

Q-switched technology is an effective approach for pulse generation of short pulse duration and high peak power. However, all reported solar-pumped passive Q-switched lasers have demonstrated output pulse widths in the hundreds of nanoseconds range. H. Arashi proposed a solar-pumped acousto-optic Q-switched laser based on heliostat and parabolic mirror, with 100 ns pulse duration at 1 kHz in 1993 [5]. In 1997, a solar pumped passively Q-switched laser (PQL) was demonstrated based on a three-stage concentrator. 3-10 Fresnel parabolic heliostats, a 3D-CPC and a 2D-CPC make up the solar concentrator. A pulse width of 180 ns was obtained with Cr^{4+}:YAG [6]. In 1999, M. Lando demonstrated a solar-pumped PQL with a similar concentrator system of Ref. 6 when the Cr^{4+}:YAG was employed as the Q-switch element, the maximum repetition rate and minimum pulse width were 48 kHz and 250 ns [7]. In 2000, M. Lando proposed a solar-pumped PQL based on Cr^{4+}:YAG, and the minimum pulse width was 190 ns [8].

Owing to the excellent properties of SCF, passively Q-switched SCF lasers have advanced rapidly in recent years. The fabrication technologies of SCF primarily employ laser heated pedestal growth, edge-defined film-fed growth and micro-pulling-down [9]. A shorter pulse width is one development goal of passively Q-switched SCF lasers. The short cavity length and the high pump power can narrow the pulse width [10-11]. The pulse width of ~ns and several hundred ps has been obtained [12-14]. H. Xia reported a pulse width of 10 ns using a SCF (Φ0.8×15 mm) [15]. Y. Cai used a SCF (Φ0.8×20 mm) to obtain a pulsed laser output with a pulse width of 104.6 ns when the absorbed pump power was only 13 W [16]. D. Wang demonstrated a pulse width of 10.6 ns for pulsed laser output from a SCF (Φ1×50 mm) laser [17].

In fact, the output pulse performance of PQLs also depends on the selection of saturable absorbers (SA) directly. Usually, crystals doped with transition metal ions have saturable absorption properties [18-20]. Cr^{4+}:YAG has a large ground state absorption cross-section, high damage threshold, low saturated light intensity and long service life [21-22]. Compared to Cr^{4+}:YAG crystals, V^{3+}:YAG has a shorter recovery time (about 180 times smaller than Cr^{4+}:YAG), a large absorption cross- section and a high damage threshold [23-25], which makes the V^{3+}:YAG more advantage of realizing high repetition rate PQLs [26-28].

SCF is also a good choice for solar pumped lasers

due to lower nonlinear effects and higher laser damage thresholds [29-30]. In 2022, a solar pumped SCF laser based on a hollow-core reflector was reported [31]. However, due to the small diameter of the fiber, the very low concentrating efficiency of end-pumping restricts the improvement of the output power of solar-pumped fiber lasers (SPFLs). Side pumping can effectively improve the pumping area, which is an important method to enhance the output power of SPFLs [32-36].

To obtain the output pulse with several nanosecnd width, a short Nd:YAG SCF is employed as the gain medium of solar pumped PQL in this paper. By optimizing the design of a three-stage solar concentrator, the solar power absorbed by the SCF achieves 40 W based on ray tracing with TracePro software. The output laser pulse characteristics of the solar pumped PQL based on Cr^{4+}:YAG and V^{3+}:YAG are also compared by solving the rate equations. When the Cr^{4+}:YAG acts as the Q-switch element, the minimum output pulse width of 5.2 ns can be obtained. This pulse width is shorter than that of the Refs. [5-8] on solar pumped PQLs, which output pulse widths were on the order of several hundred nanoseconds.

2. Concentrator system design and optimization

In this paper, a short Nd:YAG (Φ1 mm×20 mm, and 1 at.% doping concentration) SCF is acted as the gain medium. Fig. 1 demonstrates the structure of the concentrator. The rectangular parabolic mirror, 2D-CPC and 2V-shaped reflector make up the concentrator system. The entrance of the 2V-shaped reflector coincides with the outlet of the 2D-CPC, and two reflective plates are placed at both of its ends. The SCF is located at the half height of the 2V-shaped reflector.

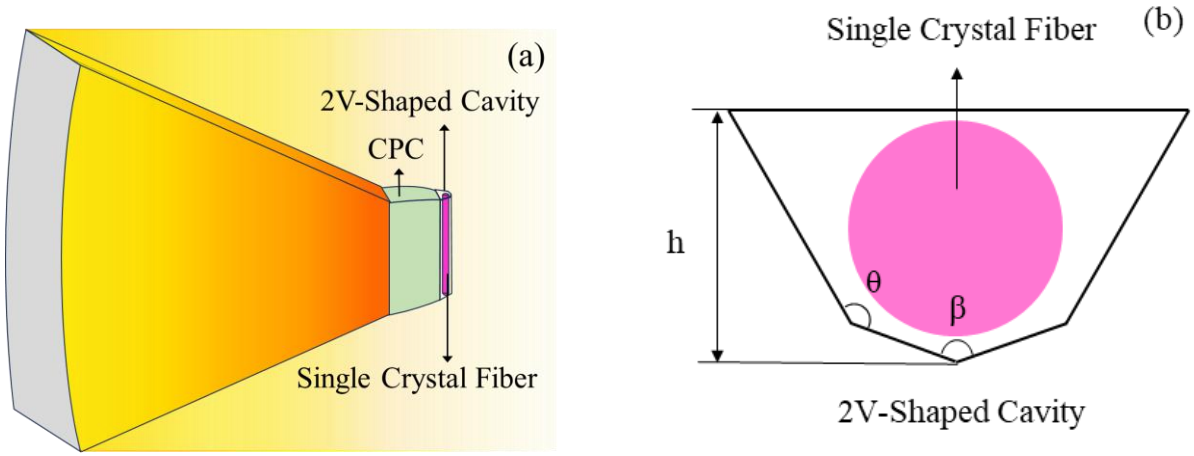

Fig. 1. Structural diagram. (a) concentrator system, (b) 2V-shaped reflector (colour online)

By cutting a rotating parabolic mirror with a focal length of 1200 mm, a rectangular parabolic reflector with a size of 2000 mm × 734 mm and an area receiving sunlight of 1.47 m^2 is obtained. The outlet size of the 2D-CPC affects the solar power absorbed by SCF. If the outlet of the 2D-CPC is too large, the entrance of the 2V-shaped reflector increases accordingly, which leads part of the sunlight entering into the 2V-shaped reflector to be reflected and escape from the entrance of reflector. On the contrary, if the outlet of the 2D-CPC is too small, it leads to the low total power of the sunlight entering the reflector. Under these two conditions, the solar power absorbed by SCF can decrease. Therefore, the outlet of the 2D-CPC is set to 20 mm × 2 mm. To improve the concentrating efficiency of the sunlight entering into the 2V-shaped reflector, it is necessary to optimize the CPC. Based on ray tracing with TracePro optical software, Fig. 2 depicts the relationship between the concentrating efficiency and the acceptance angles α_1 and α_2 in both directions of the 2D-CPC. When α_1 and α_2 are 17.5° and 65°, the CPC inlet is 6.6 mm × 22 mm, and its concentrating efficiency reaches the maximum of 59.2%. The diameter of the focal spot of parabolic mirror is about 12 mm (the FWHM of irradiance). When the CPC acceptance angle is larger, the corresponding inlet diameter of CPC is smaller than the focus size, which leads that the part of the sunlight reflected by the rectangular parabolic mirror cannot enter the 2D-CPC. When the CPC acceptance angle is small, the corresponding inlet size of CPC is much larger than the focus size, resulting in part of the sunlight escaping from the CPC inlet after reflection by the 2D-CPC, which also reduces the concentrating efficiency.

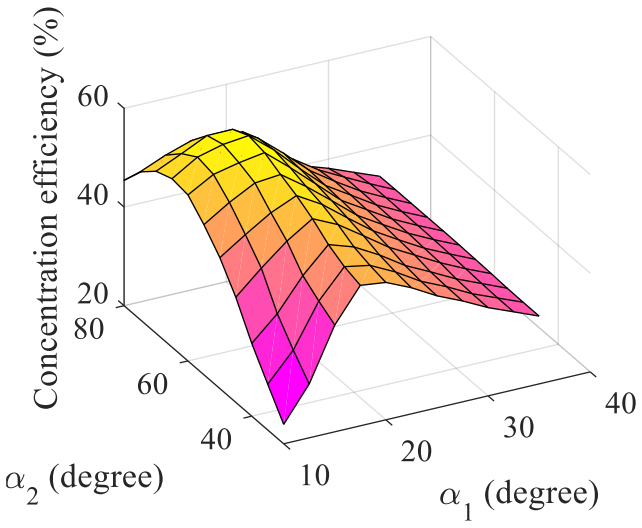

Fig. 2. Concentration efficiency of 2D-CPC versus acceptance angles α_1 and α_2 (colour online)

The height h, the two angles θ and β of the 2V-shaped reflector need to be optimized to improve the solar power absorbed by the SCF. The solar irradiance at the terrestrial surface is taken to be 1000 W/m^2 [37]. The number of rays used for tracing is about 250,000. Fig. 3 shows that solar power absorbed by the SCF depends on the h, θ and β of the 2V-shaped reflector. Ray tracing shows that the smaller the height of the reflector is, the more sunlight entering into the 2V-shape reflector can be absorbed by the SCF. When the angle β is smaller, more sunlight can be absorbed by the SCF due to the times of sunlight passing through the SCF increasing. Therefore, the height of the 2V-shaped reflector can be set to 1.1 mm. When h is 1.1 mm with $\theta = \beta = 140°$, the solar power absorbed by the SCF reaches 40 W.

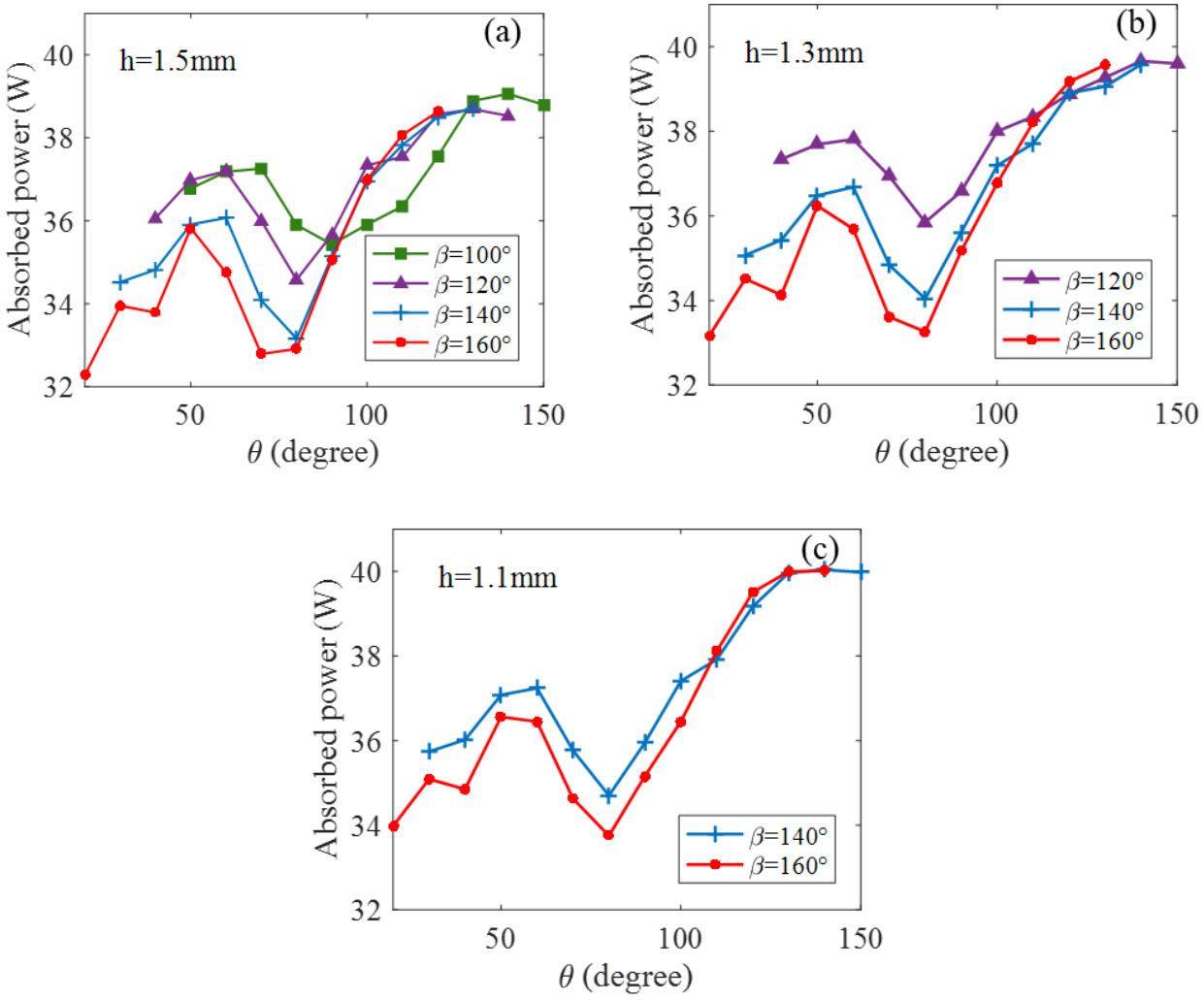

Fig. 3. The absorbed power of SCF VS the angle θ of 2V-shaped reflector (colour online)

The ambient temperature is set to 20 °C. Based on MATLAB software, the temperature distribution of the SCF along the axial and radial direction can be shown in Fig. 4. The highest temperature of 56.59 °C in the SCF is located at the position (z=12 mm), and the temperature at the end of the SCF (z=20 mm) is the lowest (37.93 °C). It is found that the SCF has the highest temperature at the core and the lowest temperature at the outer surface of SCF. The radial temperature difference at z=12 mm and 20 mm are 5.35 °C and 2.62 °C. The simulation demonstrates that the focal lengths of the SCF's thermal lens in the radial and tangential directions are 165.41 mm and 291.71 mm, respectively.

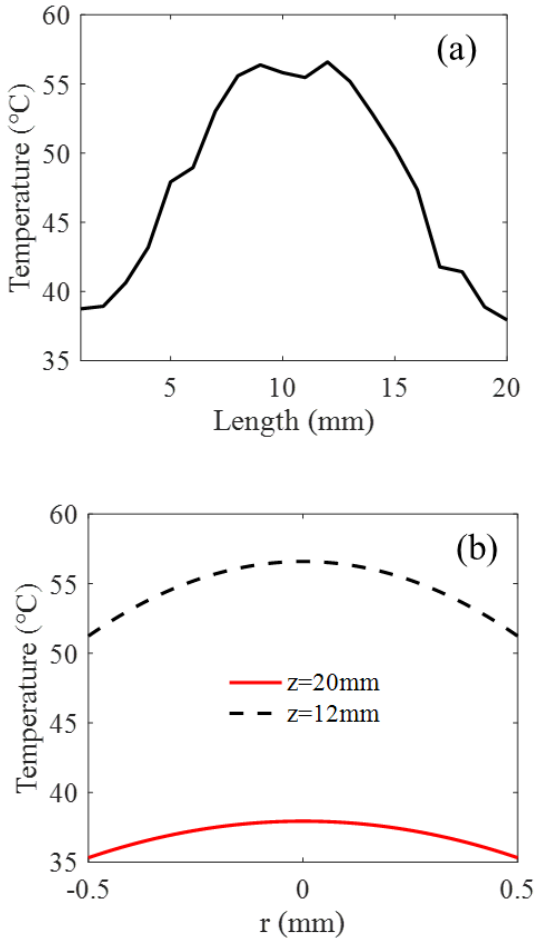

Fig. 4. Temperature distribution of SCF. (a) axial, (b) radial (colour online)

3. Simulation of laser output characteristics

The rate equations of a passively Q-switched fiber laser is [38, 39]:

$$\frac{d\phi}{dt}=\frac{\phi}{t_r}[2\sigma nl-2\sigma_{gs}n_{gs}l_s-2\sigma_{es}(n_{0s}-n_{gs})l_s -(\ln\frac{1}{R}+\delta)] \quad , \tag{1}$$

$$\frac{dn}{dt}=R_p(1-\frac{n}{N_T})-\gamma\sigma c\phi n-\frac{n}{\tau_a} \quad , \tag{2}$$

$$\frac{dn_{gs}}{dt}=\frac{n_{0s}-n_{gs}}{\tau_{gs}}-\sigma_{gs}c\phi n_{gs} \quad , \tag{3}$$

$$n_{gs}+n_{es}=n_{0s} \tag{4}$$

where ϕ is the photon density in the SCF laser cavity, and t_r is the round-trip time of light in the resonator. σ, n and l are the stimulated emission cross-section, population inversion density and length of the gain medium, respectively. σ_{gs}, n_{gs}, and l_s are the SA ground state absorption cross-section, ground state population density and length, respectively. σ_{es} is the absorption cross-section of the excited state of the SA, and n_{0s} is the total population density of the SA. R is the output coupler reflectivity, δ is the dissipative loss in the laser cavity, R_p is the pumping rate, N_T is the total population density of the gain medium. γ is the inversion factor, c is the speed of light. τ_α is the lifetime of the upper laser level of the gain medium, τ_{gs} is the recovery time of the SA, and n_{es} is the SA excited state population density.

By solving the rate equations, the single pulse energy E, pulse width Δt_p, and peak power P can be obtained through Eqs. (5)-(7) [40].

$$E=\frac{h\nu A}{2\sigma\gamma}\ln(\frac{1}{R})\ln(\frac{n_i}{n_f}) \quad , \tag{5}$$

$$\Delta t_p=\tau_c\frac{n_i-n_f}{n_i-n_t(1+\ln\frac{n_i}{n_t})} \quad , \tag{6}$$

$$P=\frac{E}{\Delta t_p} \tag{7}$$

where ν is the laser frequency (2.82×10^{14} Hz), A is the laser spot cross-section size, n_i is the initial inverted

population density, n_f is the final inverted population density, and n_t is the threshold of inverted population density.

The various parameters used for numerical simulation are shown in Tables 1-2. The length of the SCF is 20 mm. Nd:YAG SCF has five solar pumping bands of 530 nm, 580 nm, 750 nm, 810 nm and 870 nm.

Table 1. Parameters of the gain medium [41]

Parameter	Nd:YAG
stimulated emission cross-section	2.8×10^{-23} m^2
total population density	1.38×10^{26} m^3
lifetime of the upper laser level	230 μs
refractive index	1.82

Table 2. Parameters of the two SA [42-45]

Parameter	Cr^{4+}:YAG	V^{3+}:YAG
ground state absorption cross-section	7×10^{-22} m^2	3×10^{-22} m^2
excited state absorption cross-section	2×10^{-22} m^2	1.4×10^{-23} m^2
recovery time	4.1 μs	22 ns
refractive index	1.8	1.8

Fig. 5 demonstrates the relationship between the PQL's output pulse characteristics and the output coupler reflectivity (R) when the transmittance of the SA is 90%. The average wavelength of 682 nm acts as the pump wavelength.

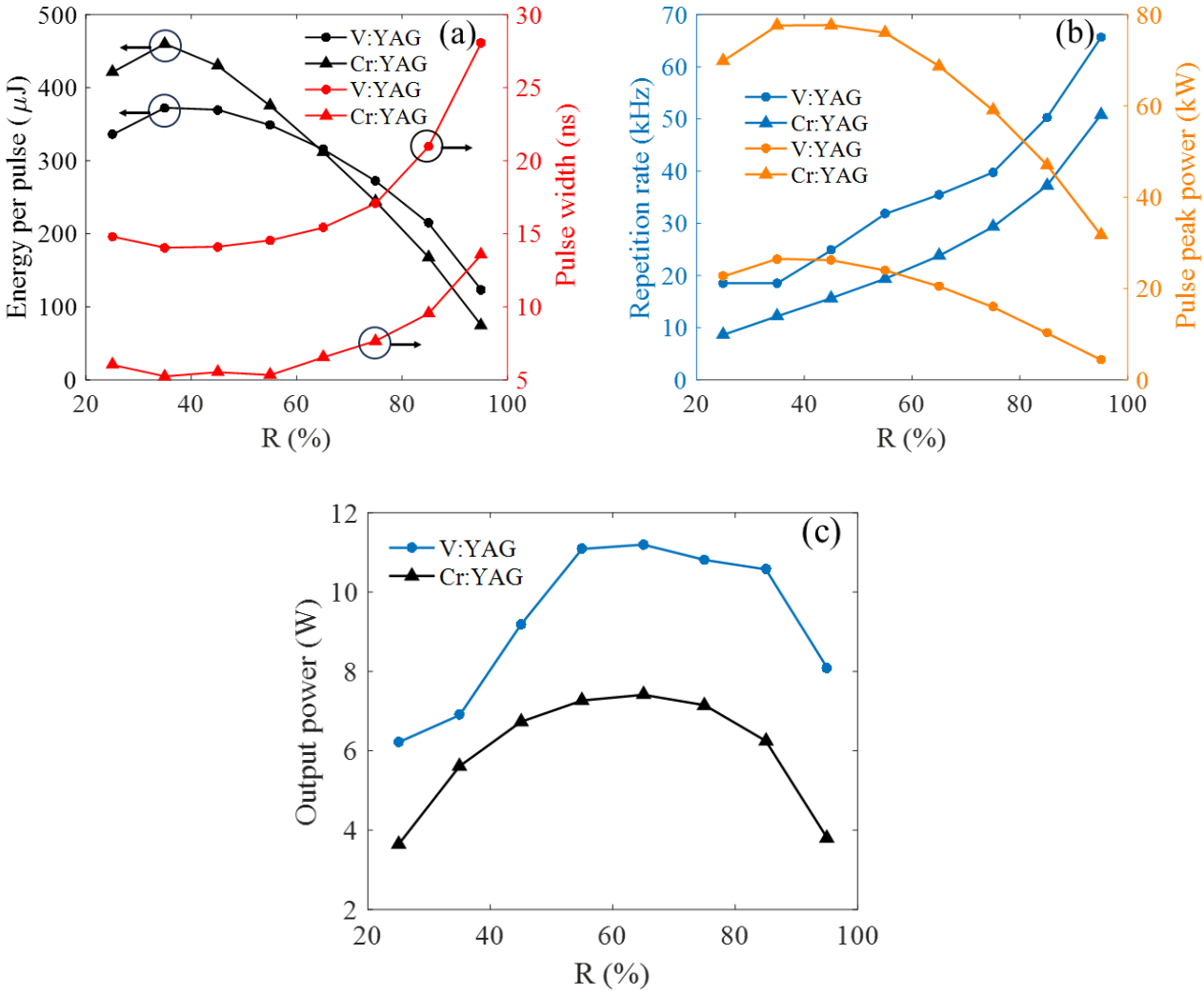

Fig. 5. Laser output characteristics varies with R. (a) single pulse energy and pulse width, (b) repetition rate and pulse peak power, (c) output power (colour online)

The maximum average output power of V^{3+}:YAG-based PQL is 11.2 W, which is higher than that of Cr^{4+}:YAG-based PQL. Fig. 5(a) depicts that there is the minimum pulse width with R increasing, which causes the decrease of the cavity loss, and the time interval for the SA to be successively "bleached" is shortened. Maximum energy and peak power of output pulse are obtained when R is 35%. Fig. 5(b) depicts that the repetition rate increases with increasing of R. The reason is that the decrease of intracavity loss and the laser threshold decrease lead to the increase of repetition rate. When R is 95%, the pulse output repetition rate of the Cr^{4+}:YAG-based and V^{3+}:YAG-based Q-switched laser are 50.7 kHz and 65.6 kHz, respectively. Since the V^{3+}:YAG recovery time is much shorter than that of Cr^{4+}:YAG, resulting in less loss induced in the cavity, the V^{3+}:YAG-based laser has higher output repetition rate than that of Cr^{4+}:YAG-based laser.

When the SA transmittance and R are 90% and 35%, Fig. 6 indicates that the individual pulse shapes of PQL based on Cr^{4+}:YAG and V^{3+}:YAG have minimum pulse widths of 5.2 ns and 14.1 ns, respectively, with corresponding repetition rates of 12.2 kHz and 18.5 kHz.

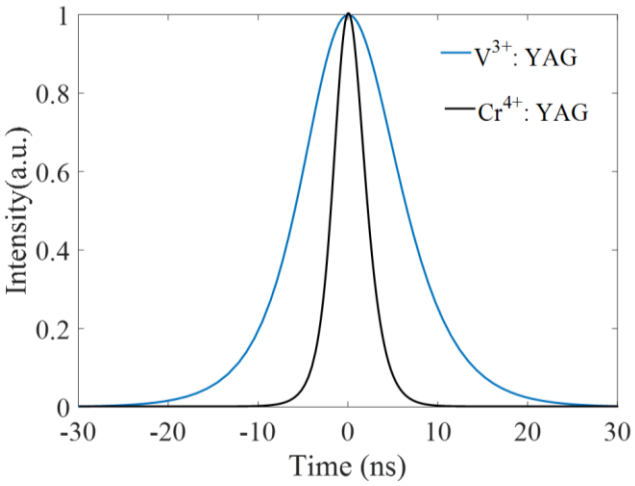

Fig. 6. Q-switched pulse shape (colour online)

4. Conclusion

To obtain the several-nanosecond pulse, a solar-pumped PQL based on a short SCF (Φ1 mm × 20 mm) is proposed. The solar concentrating system consists of a rectangular parabolic reflector (area receiving sunlight of 1.47 m^2), 2D-CPC (the outlet is 20 mm × 2 mm, two acceptance angles are 17.5° and 65°), and 2V-shaped reflector (h=1.1 mm, θ=β=140°). The short SCF can narrow the pulse width effectively. By Ray tracing with TracePro, it is found that the solar power absorbed by 20 mm SCF reaches 40 W. The laser pulse output characteristics are discussed when Cr^{4+}:YAG and V^{3+}:YAG act as Q-switching elements. Numerical simulation shows that the use of Cr^{4+}:YAG results in narrower output laser pulse width, and higher peak power than that of V^{3+}:YAG, but the output pulsed laser repetition rate is lower. When the initial transmittance of the Cr^{4+}:YAG is 90% and R =35%, the output pulse width of solar-pumped PQL is 5.2 ns. This pulse width is shorter than that of the Refs. [5-8] on solar pumped PQL, which output pulse widths were on the order of several hundred nanoseconds.

Disclosures

The authors declare no conflicts of interest.

Acknowledgment

This work is supported by Research Fund of China Three Gorges University (SDHZ2022369).

References

[1] T. Saiki, S. Taniguchi, K. Nakamura, Y. Iida, Electr. Eng. Jpn. **199**(2), 3 (2017).
[2] S. Berwal, N. Khatri, D. Kim, Appl. Surf. Sci. Adv. **12**, 100348 (2022).
[3] H. Qi, L. Lan, Y. Liu, P. Xiang, Y. Tang, Curr. Opt. Photon. **6**(6), 627 (2022).
[4] M. Küblböck, J. Will, H. Fattahi, APL Photonics **9**(5), 050903 (2024).
[5] H. Arashi, Y. Kaneda, Sol. Energy **50**(5), 447 (1993).
[6] I. Peer, N. Naftali, D. Abramovic, Y. Noter, A. Yogev, M. Lando, Y. Shimony, Proc. SPIE **3092**, 273 (1997).
[7] M. Lando, Y. Shimony, R. M. J. Benmair, D. Abramovich, V. Krupkin, A. Yogev, Opt. Mater. **13**(1), 111 (1999).
[8] M. Lando, Y. Shimony, Y. Noter, R. M. J. Benmair, A. Yogev, Appl. Optics **39**(12), 1962 (2000).
[9] P. Gu, P. Wang, W. Guan, L. Zheng, Y. Tan, J. Synth. Cryst. **50**(12), 2362 (2021).
[10] O. Schmidt, J. Rothhardt, F. Röser, S. Linke, T. Schreiber, K. Rademaker, J. Limpert, S. Ermeneux, P. Yvernault, F. Salin, A. Tünnermann, Opt. Lett. **32**(11), 1551 (2007).
[11] Y. Tang, Y. Yang, J. Xu, Y. Hang, Opt. Commun. **281**(22), 5588 (2008).
[12] Y. Zhou, M. Jiao, T. Lian, J. Xing, Y. Liu, J. Liu, Chin. J. Lasers **45**(12), 1201008 (2018).
[13] H. Lin, X. Huang, H. Liu, Optik **207**, 163831 (2020).
[14] J. Tang, Y. Qi, Z. Bai, Y. Qi, J. Ding, B. Yan, Y. Wang, Z. Lyu, Chin. J. Quantum. Electron. **40**(4), 483 (2023).
[15] H. Xia, Y. Yao, Z. Li, Laser Technol. **30**(5), 541

(2006).
[16] Y. Cai, B. Xu, Y. Zhang, Q. Tian, X. Xu, Q. Song, D. Li, J. Xu, I. Buchvarov, Photonics Res. **7**(2), 162 (2019).
[17] D. Wang, X. Liu, Y. Lai, L. Qin, W. Liang, F. Ruan, C. Yang, X. Chen, X. Rong, Infrared Phys. Technol. **136**, 105113 (2024).
[18] B. Xu, Y. Cheng, Y. Wang, Y. Huang, J. Peng, Z. Luo, H. Xu, Z. Cai, J. Weng, R. Moncorgé, Opt. Express **22**(23), 28934 (2014).
[19] X. Wang, Y. Wang, D. Mao, L. Li, Z. Chen, Opt. Mater. Express **7**(8), 2913 (2017).
[20] J. Wang, Y. Wang, T. Wang, S. Liu, H. Wang, T. Dong, Y. Wang, IEEE Photonics Technol. Lett. **32**(1), 3 (2020).
[21] M. E. Jazi, M. D. Baghi, M. Hajimahmodzadeh, M. Soltanolkotabi, Opt. Laser Technol. **44**(3), 522 (2012).
[22] J. Tang, Z. Bai, D. Zhang, Y. Qi, J. Ding, Y. Wang, Z. Lu, Photonics **8**(4), 93 (2021).
[23] Y. Li, S. Zhao, Y. Sun, H. Qi, G. Zhang, Opt. Eng. **49**(12), 124202 (2010).
[24] J. Xu, H. Huang, J. He, J. Yang, B. Zhang, X. Yang, F. Liu, Appl. Phys. B-Lasers Opt. **103**(1), 75 (2011).
[25] X. Li, X. Gao, J. Xu, S, Liu, X. Yang, Laser Phys. **21**(10), 1755 (2011).
[26] X. Zhang, P. Loiko, J. M. Serres, V. Jambunathan, Z. Wang, S. Guo, A. Yasukevich, A. Lucianetti, T. Mocek, U. Griebner, V. Petrov, X. Xu, M. Aguoló, F. Díaz, X. Mateos, Appl. Optics **57**(28), 8236 (2018).
[27] B. Wang, H. Yu, H. Zhang, Laser Phys. Lett. **16**, 015801 (2019).
[28] C. Zhu, H. Lin, R. Mu, M. Wang, F. Xiong, J. Russ. Laser Res. **43**(4), 482 (2022).
[29] Y. Zhao, L. Wang, W. Chen, J. Wang, Q. Song, X. Xu, Y. Liu, D. Shen, J. Xu, X. Mateos, P. Loiko, Z. Wang, X. Xu, U. Griebner, V. Petrov, High Power Laser Sci. Eng. **8**, e25 (2020).
[30] B. Liu, P. R. Ohodnicki, Adv. Mater. Technol. **6**, 2100125 (2021).
[31] P. Xiang, L. Lan, Y. Liu, H. Qi, Y. Tang, X. Ma, Appl. Optics **61**(28), 8988 (2022).
[32] P. Guo, M. Ou, Y. Liu, Y. Tang, J. Zhou, L. Lan, Optik **247**, 167933 (2021).
[33] P. Guo, J. Zhang, Z. Chen, L. Lan, Y. Liu, Y. Tang, X. Ma, Optik **271**, 170096 (2022).
[34] J. Zhu, Y. Liu, L. Lan, Y. Tang, Y. Zhang, X. Ma, Laser Phys. Lett. **20**(12), 125101 (2023).
[35] T. Saiki, S. Uchida, K. Imasaki, S. Motokoshi, M. Nakatsuka, AIP Conf. Proc. **702**, 378 (2004).
[36] S. Payziyev, A. Sherniyozov, A. Qakhkhorov, J. Photon. Energy **14**(2), 024502 (2024).
[37] C. R. Vistas, D. Liang, D. Garcia, B. D. Tibúrcio, J. Almeida, Appl. Sol. Energy **56**(6), 449 (2020).
[38] J. J. Degnan, IEEE J. Quantum Electron. **31**(11), 1890 (1995).
[39] J. Dong, Opt. Commun. **226**, 337 (2003).
[40] Z. Xiong, L. Jiang, T. Cheng, H. Jiang, Chin. J. Lasers **50**(6), 0601001 (2023).
[41] W. Koechner, Solid-State Laser Engineering, Springer, New York, America, 48, 2005.
[42] A. M. Malyarevich, I. A. Denisov, K. V. Yumashev, R. S. Conroy, B. D. Sinclair, Appl. Phys. B-Laser Opt. **67**, 555 (1998).
[43] J. Xu, H. Huang, J. He, J. Yang, B. Zhang, C. Zuo, X. Yang, S. Zhao, Opt. Mater. **32**, 522 (2010).
[44] Z. Burshtein, P. Blau, Y. Kalisky, Y. Shimony, M. R. Kokta, IEEE J. Quantum Electron. **34**(2), 292 (1998).
[45] C. Yang, Q. Chen, K. Xiong, X. Yin, Y. Huo, Laser & Infrared **33**(1), 21 (2003).

*Corresponding authors: 240014775@qq.com
liuyan703@163.com